

Supporting Information

Guidelines for Designing Highly Concentrated Electrolyte for Low Temperature Applications

Guillaume Ah-lung,^a Benjamin Flamme,^a Fouad Ghamouss,^{a,b} Manuel Maréchal,^c and Johan Jacquemin,^{*a,b}

- Laboratoire PCM2E, Université de Tours, Parc de Grandmont, 37200 Tours, France.
E-mail: jj@univ-tours.fr
- Materials Science and Nano-engineering (MSN) Department. Mohammed VI Polytechnic University (UM6P), Lot 660 – Hay Moulay Rachid, 43150, Benguerir, Morocco.
- Université Grenoble Alpes, IRIG-SyMMES, 38000 Grenoble, France.

Table of contents:

<i>Small- and Wide-Angle X-ray Scattering (SWAXS)</i>	S2
<i>Electrochemical analysis</i>	S3
<i>Electrolyte preparation and behavior</i>	S3
<i>DSC measurements</i>	S5
<i>LiTFSI 21m, a Temperature Story</i>	S7
<i>Miscellaneous figures</i>	S10
<i>References</i>	S11

Small- and Wide-Angle X-ray Scattering (SWAXS)

Variable temperature Small- and Wide- Angle X-ray scattering measurements were performed using a Xenocs setup equipped with a Mo GENIX anode over a large q -range from 0.4 to 25 nm⁻¹. The K_α radiation ($\lambda = 0.071$ nm) is selected using multilayered curved mirrors focusing the beam toward infinity. The size of the beam at the sample position (0.8 x 0.8 mm²) is defined by two sets of scatterless FORVIS slits. The scattered beam was recorded using a large online scanner detector (345 mm in diameter from MAR Research) located at 748 mm from the sample. Sample and empty cell transmissions are determined using an offline pin diode that can be inserted downstream from the sample. Silver behenate (AgBe, CAS number: [2489-05-6]) was used for the q -range calibration of the 2D detector. Quartz capillaries (2 mm in diameter with a wall thickness of 0.01 mm) from Hilgenberg were used as sample containers. The contribution of the empty capillary was subtracted from the scattering intensity of the studied samples. 2D images were converted into radial averages over the image centre to yield the scattered intensity $I(q)$ vs. scattering-vector modulus q using the [Datasqueeze](#) software. The scattered intensities are expressed as a function of q , the scattering vector, and $q = (4\pi/\lambda) \cdot \sin(\theta/2)$, where λ is the wavelength of the incident beam, and θ the scattering angle. The intensity curves were scaled to the absolute intensities with the aid of a laboratory-calibrated Lupolen[®] sample. The experimental resolution is $\Delta q/q = 0.05$. For temperature-resolved measurements, samples were subjected to a heating/cooling rate of 1°C·min⁻¹ and equilibrated for 2 minutes at each temperature before data acquisition of 2000 s. In the same way as described in the electrolyte preparation section, LiTFSI salt (extra dry, <20 ppm, Solvionic) was evaluated to contain a maximum of (30 ± 5) ppm of water by Karl-Fisher titration (899 Titrand, Metrohm), and was stored in an argon-filled glove box. Sealed vials were filled inside before making aqueous solutions to fill capillaries.

Electrochemical analysis

Cyclic voltammetry (CV) measurements were performed in a 2-electrode configuration using coin cell (CR-2032) with activated carbon-based electrodes (10 mm in diameter) coated on aluminum current collectors from Samwha Capacitor. These electrodes were composed of 85 wt.% of activated carbon as active material, and 15 wt.% of additives with a total mass loading of $7 \text{ mg}\cdot\text{cm}^{-2}$. These electrodes are separated from each other by a GF/C type Whatman® glass microfiber filters punched at 16 mm diameters and soaked with 100 μL of electrolyte. Sealed coin cells were connected to a VMP3 type potentiostat/galvanostat from Biologic. Channel cables were entered in a dynamic climate chamber (Binder MK056) through dedicated access and subsequently isolated by glass wool. The climate chamber was set at the targeted temperature ($\pm 0.1 \text{ }^\circ\text{C}$) and a stabilization time of 2 h was used before running each experiment ensuring that all the system (coin cell, electrolyte, *etc.*) reached the operating temperature.

Electrolyte preparation and behavior

For other measurements than those run with the SWAXS, the lithium bis[(trifluoromethyl)sulfonyl]imide (LiTFSI, 99%; water content = $30 \pm 5 \text{ ppm}$) purchased from Fluorochem was used. The bottle was opened and stored in an argon filled glove box (MBraun, model number: MB-200B) with a water level always below 5 ppm. Ultrapure water ($18.2 \text{ M}\Omega\cdot\text{cm}$) was freshly obtained from a Milli-Q™ water purification system. In order to avoid a maximum of moisture contamination (**Fig. S1a**), a glass vial with a stirrer, both previously dried, were introduced into the glove box. The appropriate amount of LiTFSI, by considering its residual water level, was then weighted on a Sartorius 1602 MP balance (with $\pm 10^{-4} \text{ g}$) and the vial was closed and took out from the glove box. Immediately after, the water, previously weighted, was introduced to the vial and the mixture was stirred. Uncertainty in the LiTFSI-based electrolytes composition was estimated to be better than $u(x_{\text{LiTFSI}}) = 2 \cdot 10^{-4}$.

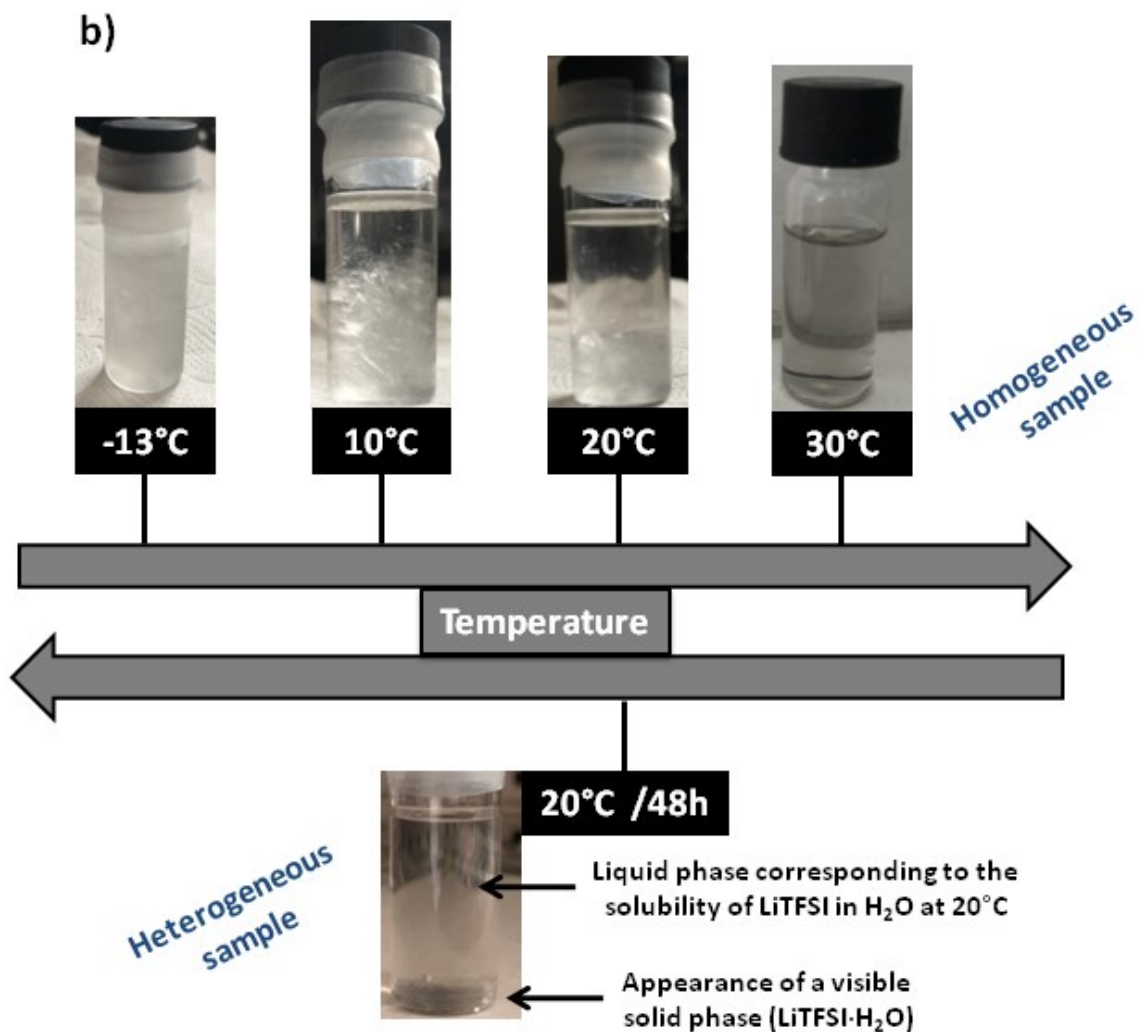
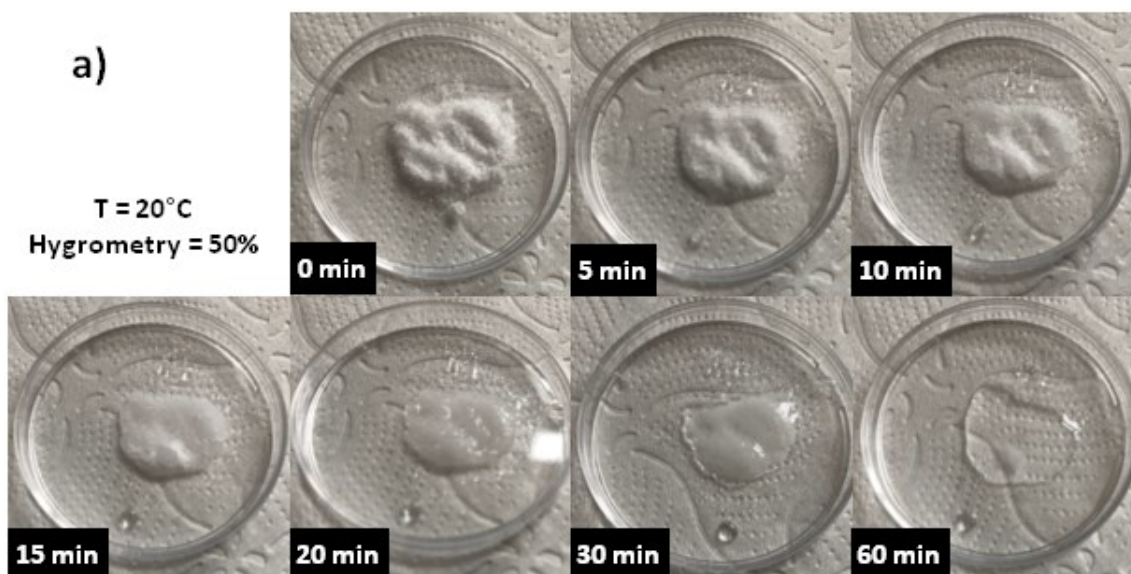


Fig. S1: Illustration of the moisture contamination on dry LiTFSI (300 mg) extracted from our glove box (a), LiTFSI 21m appearance at key temperatures (b).

In **Fig. S1b**, the slow appearance of a solid phase during the storage at 20 °C clearly demonstrate the coexistence of a liquid and a solid phases of different water:LiTFSI compositions. Of course, in the case of the LiTFSI 21m electrolyte, this phases coexistence must be seen in the range of temperature between its *solidus* and *liquidus*. The use of electrochemical devices filled with LiTFSI 21m on this temperature range will generate an inhomogeneous electrolyte, which could induce thus the deposition of the generated solid phase onto the surfaces of the separator and/or electrodes leading to a potential system failure or shutdown.

Lithium nitrate (LiNO₃, BioUltra, > 99.0%, water content = 4700 ± 200 ppm) was purchased from Sigma Aldrich. The appropriate amount of LiNO₃ (corresponding to 24.5 wt.%) is dissolved in freshly obtained ultrapure water (18.2 MΩ·cm) by considering the residual water level in the LiNO₃ salt. The mixture was stirred for 1 h at 20 °C and punctually heated (< 40 °C) ensuring adequate homogeneity of the electrolyte. The vial was stored in a dried environment and DSC measurements were performed before each utilization verifying the right composition. Uncertainty in the eutectic composition was estimated to be better than $u(w_{\text{LiNO}_3}) = 0.1 \text{ wt.}\%$.

DSC measurements

DSC scans were performed on a Perkin Elmer DSC 4000 under a continuous nitrogen flow (20 mL min⁻¹), coupled with an Intracooler SP VLT100. Samples were introduced in 40 μL single use aluminum crucibles and then cold sealed with an adapted press. Temperature scan rate was defined at 2°C·min⁻¹ with an initial stabilization time of 5 min. Uncertainty of the reported phase transition temperatures, estimated thanks to the eutectic temperature of the LiNO₃-water binary mixture, is close to $u(T) = 0.1 \text{ }^\circ\text{C}$. A variety of Whatman® glass microfiber separators were investigated with LiNO₃ based electrolytes. Their porosities are as follow: GF/A = 1.6 μm, GF/C = 1.2 μm, GF/D = 2.7 μm, GF/F = 0.7μm.

To avoid any ambiguous information that can occur during the exploitation of DSC thermograms, recommendations and advices reported in the literature were followed,^{S1-S3} as briefly described below. As reported by Ferreira *et al.*,^{S1} a very broad melting peak leading to a large difference between the *solidus* and the *liquidus* is especially seen for a composition near to a well-defined congruent melting crystal solvate and to a peritectic point.^{S2} That is why a short reminder in DSC interpretation is described in **Fig. S2** and below based on the LiTFSI 21m sample ($T_{\text{preparation}}$ and $T_{\text{storage}} > 25 \text{ }^\circ\text{C}$).

Determination of the lower limit of LiTFSI 21m liquid state window: As described by Garidel *et al.*,^{S3} using the onset/endpoint or the tangent method to determine the *solidus* and the *liquidus* is only accurate for the latter. To solve this, Ferreira *et al.* proposed that "the first shift from the baseline before the peak in the heating path can be considered the best estimate of the *solidus*".^{S1} This proposition was used in this paper (Fig. S2), in our hands the *solidus* was determined at -15 °C and the *liquidus* at 27 °C. It means that both a solid and a liquid phase are coexisting between these two limits leading to a large heterogenous temperature region about 42 °C. As the composition of the liquid phase is directly dependent on the temperature driven by its LiTFSI solubility, leading to a "metastable composition" region, a homogenous liquid electrolyte with a LiTFSI 21m composition cannot be used under its *liquidus* temperature, *i.e.* 27 °C. Considering that, *in fine* performances will be altered by the coexistence of a solid phase (of the composition of the incongruent melting LiTFSI·H₂O crystal by looking at the phase diagram available in ref. [S2]) caused by a decrease in salt concentration into the liquid phase electrolyte for any temperature range from its *solidus* and *liquidus*.

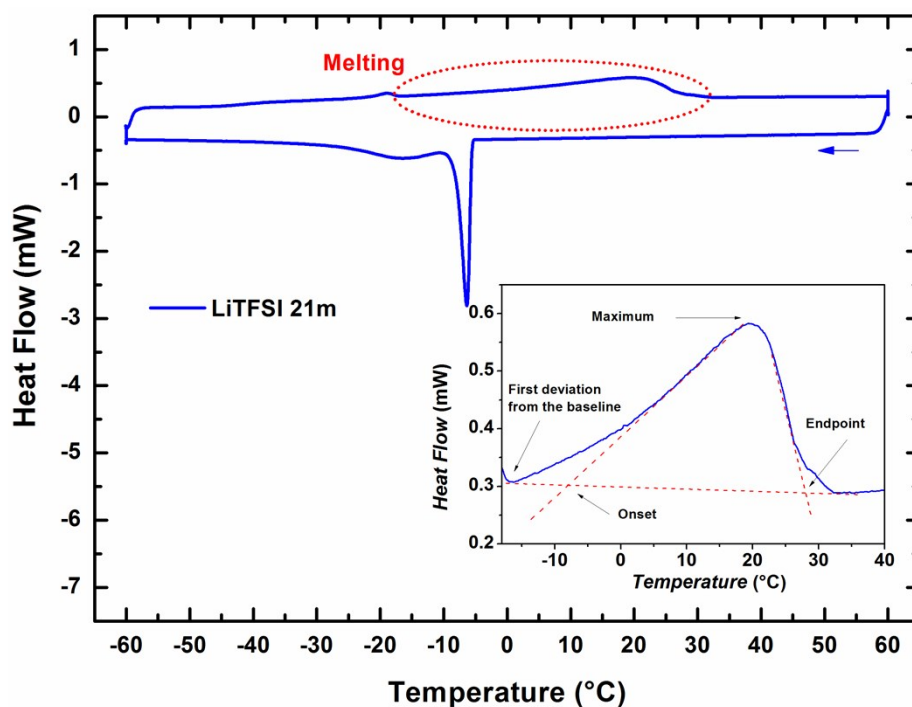


Fig. S2: Typical DSC trace of LiTFSI 21m, the inset is a magnification of melting region to explicit the *solidus* and the *liquidus* determination

LiTFSI 21m, a Temperature Story

Not a long time ago, in a laboratory not so far away, differences in thermograms were observed, during DSC preliminary studies, for the same electrolytes depending on the temperature of the preparation room. Crystallization peaks were observed at $-3\text{ }^{\circ}\text{C}$ (**Fig. S3a**, green curve) when the preparation temperatures were above $25\text{ }^{\circ}\text{C}$, however during colder days, another batch of electrolytes was prepared when temperature were below $20\text{ }^{\circ}\text{C}$, crystallization peaks appears at $-48\text{ }^{\circ}\text{C}$ during DSC scans (**Fig. S3a**, blue curve) and this, in both cases, with macroscopically homogeneous electrolytes. This clearly demonstrates that each scientific paper must simply ban the use of the term “room temperature”, which does not have any scientific meaning. Moreover, when this "cold" electrolyte was heated at $50\text{ }^{\circ}\text{C}$ during the DSC scan, the crystallization peak return back to the previous value (e.g. $-3\text{ }^{\circ}\text{C}$, **Fig. S3a**, red curve).

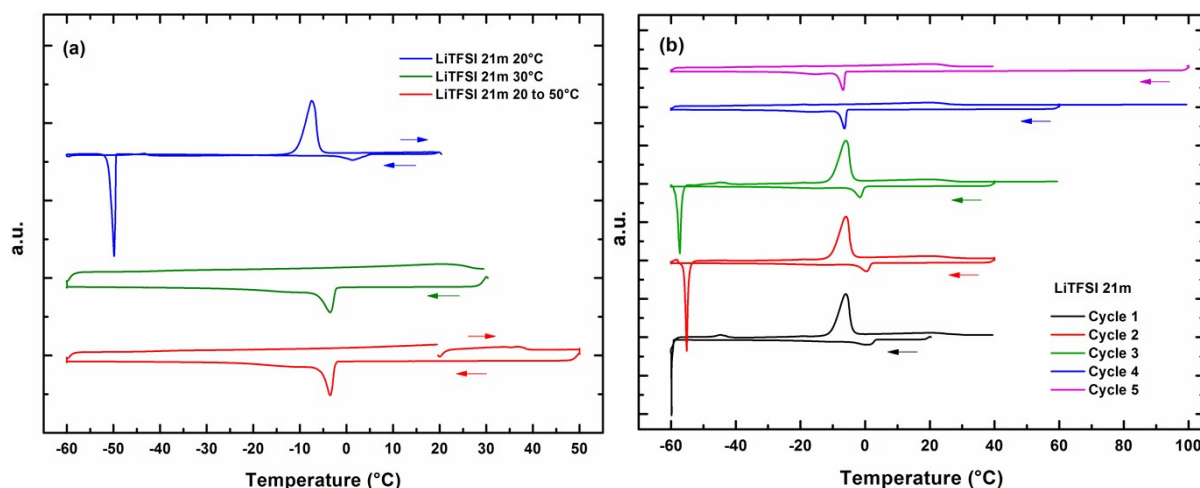


Fig. S3 DSC thermograms of LiTFSI 21m on either side of the activation barrier (a), and successive DSC cycles crossing the activation barrier (b).

Those results appear as the existence of an “activation barrier” between a purely liquid ($x_{\text{LiTFSI}} = 0.275$) and a more diluted solution ($x_{\text{LiTFSI}} < 0.275$) containing LiTFSI·H₂O solid micro-domains ($x_{\text{LiTFSI}} = 0.5$) leading to a larger liquid state window in the DSC trace. This last proposition was confirmed by the following experiment. During multiple day storage below $20\text{ }^{\circ}\text{C}$, the initially homogeneous electrolytes have separated into a solid crystalline phase and a liquid supernatant. The DSC analyses of this less concentrated liquid phase ($x_{\text{LiTFSI}} < 0.275$) show an extended liquid state window as expected (**Fig. S4**).

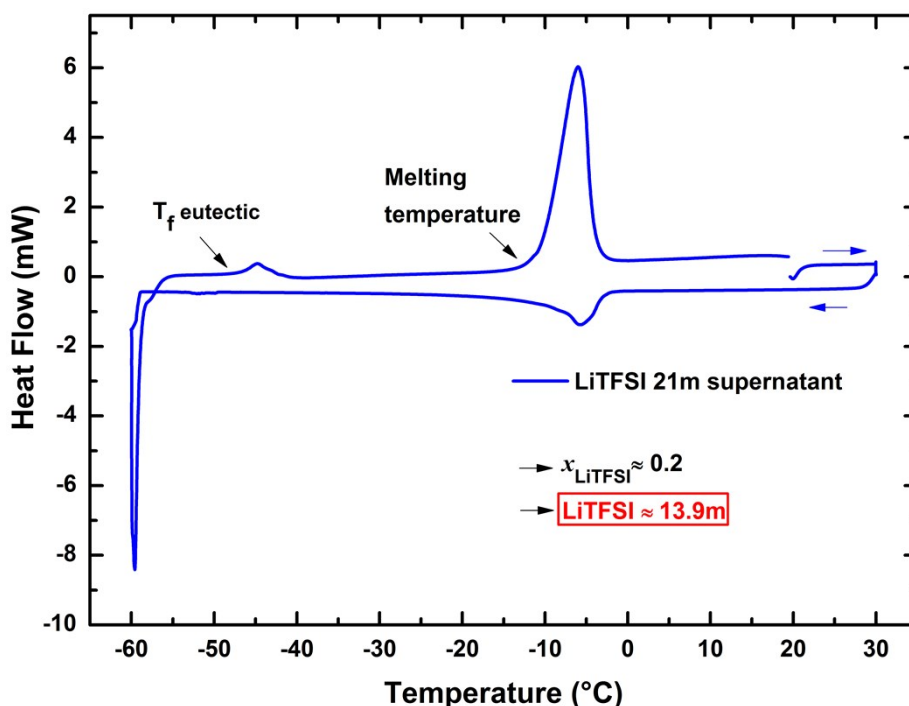


Fig. S4 DSC thermogram of the supernatant obtained from inhomogeneous LiTFSI 21m stored below 25 °C. The melting temperature is closed to that of the congruent melting of LiTFSI·(H₂O)₄.

According to thermal studies (**Fig. S3 and S4**) and the phase diagram of LiTFSI/water binary mixture,^{S2} from 21m composition the only possibility for decreasing the crystallization temperature, *i.e.* corresponding to a lowering of the melting temperature, is to decrease the salt concentration which can be achieved by using the supernatant of heterogeneous LiTFSI 21m (stored below 25°C). However, the supernatant concentration is not 21m anymore. **Fig. S4** shows the corresponding thermal analysis of the supernatant and as expected, the global trace is far away from a “true” LiTFSI 21m. As the eutectic fusion peak, as well as, a fusion peak near to the congruent melting of LiTFSI·(H₂O)₄ crystal, phase diagram available in ref. [S2], are visible on the DSC trace, it is clear that the LiTFSI molar fraction of the supernatant is shifted to lower LiTFSI molar fractions on the binary phase diagram of LiTFSI/water.^{S2} The only one possibility is obtained with a x_{LiTFSI} close to 0.2 (13.9m), equivalent to a 33% drop in the concentration.

To continue within this approach, a DSC pan containing a homogenous LiTFSI 21m electrolyte was prepared and then stored at 20 °C, so below its normal melting temperature. This electrolyte has then undergone successive DSC cycles with a positive gradient for the consecutive starting temperatures, as shown in **Fig. S3b**. The first cycle, (black curve in **Fig. S3b**) starting at 20 °C and ending at 40 °C, is similar to the DSC trace done with the sample prepared at 20 °C (**Fig. S3a** blue curve) with a first crystallization peak right shifted at 5 °C

while the second crystallization peak is shifted to lower temperature ($-60\text{ }^{\circ}\text{C}$), while the well-defined corresponding fusion peak ($-13\text{ }^{\circ}\text{C}$) is still observed at the same temperature. The second fusion peak is visible here as a broad shoulder ending close to $27\text{ }^{\circ}\text{C}$. During the second and the third cycles, slight deviations from the previously described peaks appeared. Nonetheless, when the electrolyte was then heated from $40\text{ }^{\circ}\text{C}$ to $60\text{ }^{\circ}\text{C}$ or even $100\text{ }^{\circ}\text{C}$ (**Fig. S3b**), the first crystallization peak has returned to $-3\text{ }^{\circ}\text{C}$ with the corresponding broad fusion peak ending around $27\text{ }^{\circ}\text{C}$, comparable to that observed in phase diagrams available in the literature.^{S2,S4} This was further evaluated using SWAXS measurements, revealing q reflections due to the crystalline phase up to $18\text{ }^{\circ}\text{C}$ (**Fig. S5**), and confirming the presence of a crystalline state up to at least $18\text{ }^{\circ}\text{C}$. The anhydrous LiTFSI is crystallized in an orthorhombic phase^{S5} and the obtained pattern seems to be the shifted pattern to higher q , *i.e.* larger characteristic distances. The large broad peaks around 1.0 and 1.5 \AA^{-1} , convolved with the reflections, are attributed to a pure liquid phase permanently and concomitantly present in the temperature range of the experiment. However, according to the SWAXS patterns, depending on the storage temperature, this solution could contain two sub-phases (solid and liquid) coexisting at temperature below its normal melting point.

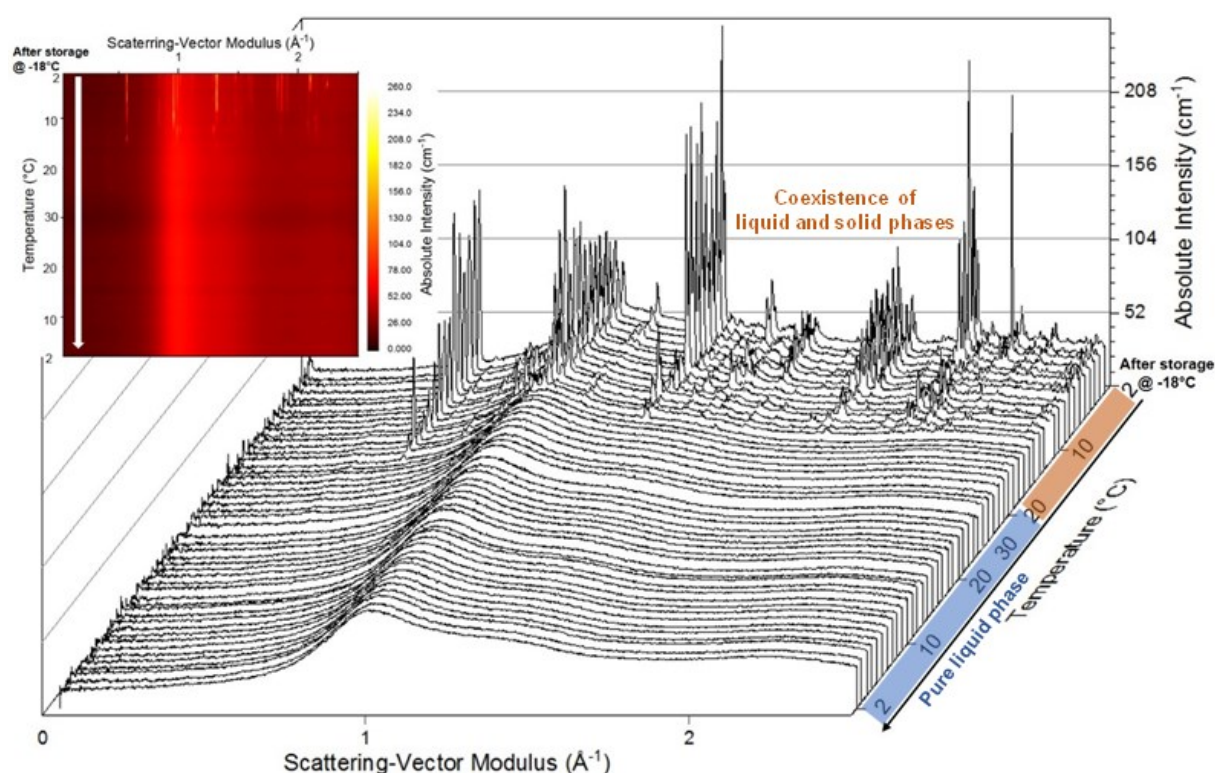


Fig. S5 SAXS/WAXS 2D (inset) and 3D patterns of the LiTFSI 21m as a function of the temperature. SAXS/WAXS scattering was performed, after storing at $-18\text{ }^{\circ}\text{C}$, upon heating (from 2 up to $30\text{ }^{\circ}\text{C}$) and then cooling (from 30 down to $2\text{ }^{\circ}\text{C}$) scans.

Furthermore, the exothermic contribution, shown in **Fig. S3b** around 0 °C, slightly shifting to the lower temperatures by heating the solution from 40 °C up to 100 °C, is due to the crystallization of this liquid (low salt concentration) sub-phase. This shift was also confirmed by SWAXS (**Fig. S5**) as no crystallization down to 2 °C is observed after heating the solution at 30 °C. In other words, this is concomitant with the reverse shift of the crystallization peak of the salt concentrated sub-phase. Indeed, these outcomes are highlighting a phase transition at a temperature located between 40 °C and 60 °C. According to solid-liquid LiTFSI-H₂O binary phase diagram available in the literature, this transition does not exist for a 21m electrolyte, but could be crossed for higher molality or high molar fraction compositions while an interesting phase change is described at around $T = 43$ °C (peritectic line).^{S2} As described before, this electrolyte was prepared and stored below its normal melting temperature, meaning that two phases are present, a liquid one with a molality inferior to 21m and a portion of H₂O·LiTFSI solid micro-domains with an obvious molar fraction of 0.5 according to ref. [S2]. These solid micro-domains can become visible after a more or less long storage period as pictured by Reber *et al.*^{S6} or by our self (**Fig. S1b**). Below 43 °C (Cycles 1 to 3) DSC curves have shown the combined response of the two phases. Above 43 °C (Cycles 4 and 5) solid micro-domains became liquid releasing an important quantity of salt, increasing the molality of the entire solution to 21m giving the true DSC curve of this solution.

Miscellaneous figures

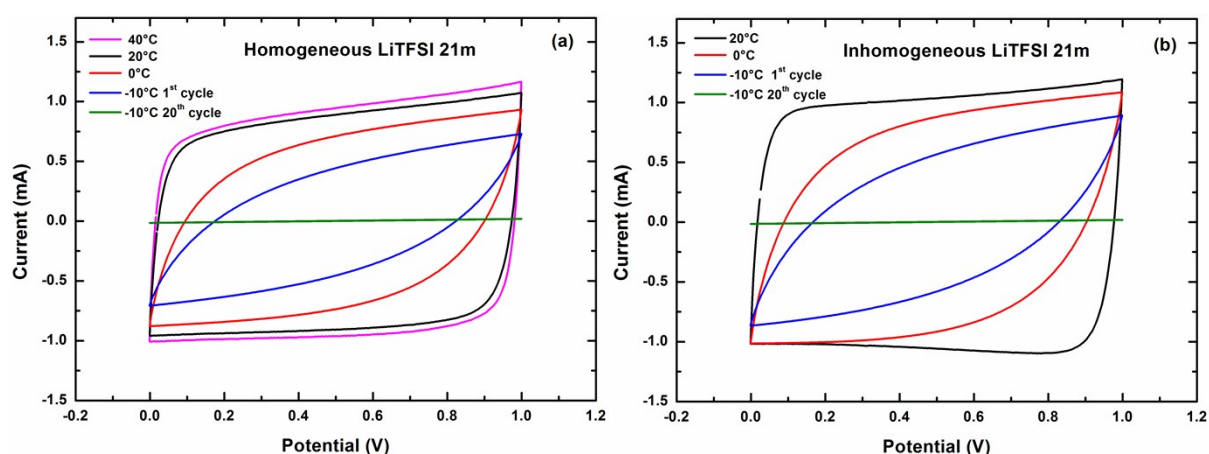


Fig. S6 Cyclic voltammograms at 10 mV·s⁻¹ of A.C.//A.C. coin cells cycled at different temperature with homogeneous electrolyte **(a)** and inhomogeneous electrolyte **(b)**.

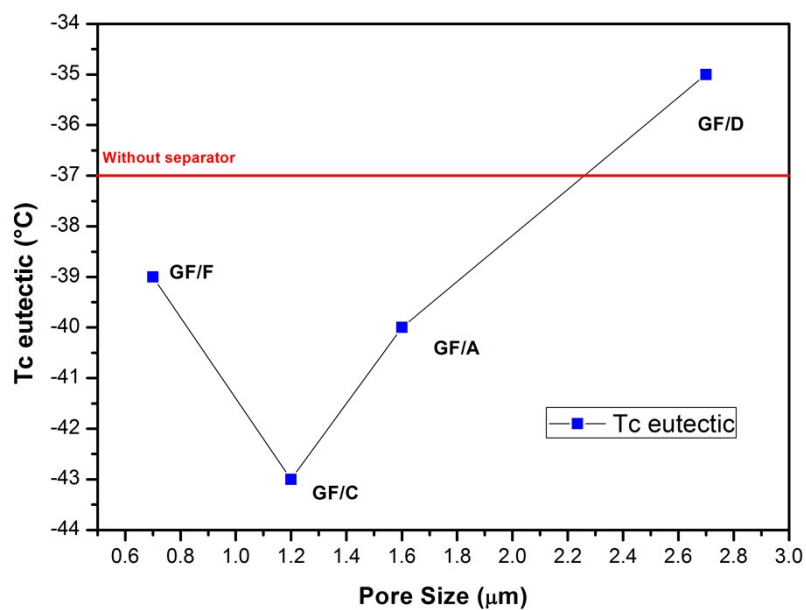


Fig. S7 Evolution of the eutectic LiNO_3 crystallization as function of the corresponding separator pore size determined by DSC

The impact of the separator on the thermal response has been shown and verified some previous hypotheses and how it is depicted in **Fig. S7** the porosity of the separator (from Whatman glass microfibers series) influenced the crystallization.

References

- [S1] E. B. Ferreira, M. L. Lima and E. D. Zanotto, *J. Am. Ceram. Soc.*, 2010, **93**, 3757-3763.
- [S2] M. S. Ding and K. Xu, *J. Phys. Chem. C*, 2018, **122**, 16624-16629.
- [S3] P. Garidel, C. Johann and A. Blume, *J. Therm. Anal. Calorim.*, 2005, **82**, 447-455.
- [S4] G. Perron, D. Brouillette and J. E. Desnoyers, *Can. J. Chem.*, 1997, **75**, 1608-1614.
- [S5] J. L. Nowinski, P. Lightfoot and P. G. Bruce, *J. Mater. Chem.*, 1994, **4**, 1579-1580.
- [S6] D. Reber, R-S. Kühnel and C. Battaglia, *ACS Mater. Lett.*, 2019, **1**, 44-51.